VIII International Conference on Particle-Based Methods
PARTICLES 2023
U. Perego, M. Cremonesi, A. Franci (Eds)

NUMERICAL INVESTIGATION OF PRESSUREMETER TEST WITH MATERIAL POINT METHOD

HARSHA VARDHAN KURUGODU[1], DEBAYAN BHATTACHARYA[1], PRASHANTH VANGLA[1] AND DAVID FROST [2]

[1] Department of Civil Engineering, Indian Institute of Technology Delhi
Hauz Khas, 110016, New Delhi, Delhi, India
e-mail: cez218277@iitd.ac.in, debayanb@civil.iitd.ac.in, pvangla05@civil.iitd.ac.in

[2]School of Civil and Environmental Engineering, Georgia Institute of Technology,
790 Atlantic Dr., Atlanta, GA 30332, USA
e-mail: david.frost@ce.gatech.edu

Abstract. In situ tests for geotechnical investigations can provide a reliable prediction of the soil behaviour because they accurately represent the stress state while preserving the soil structure and the inherent material fabric. These tests complement the information obtained from laboratory element tests on undisturbed or reconstituted specimens. The pressuremeter test is one such example of an in-situ tool that is used to obtain soil properties based on measured pressure-volume data. The pressuremeter test is considered a large deformation problem within a numerical framework. Furthermore, it is commonly idealized as a cylindrical cavity expansion within the realms of conventional finite element schemes. In order to address the issue related to excessive mesh distortion aspects, the Eulerian-Lagrangian approach developed within a continuum framework, namely the Material Point Method (MPM), has been adopted in the present study to investigate the pressuremeter expansion process. First, the results obtained are benchmarked against those from classical cavity expansion problems for a pressure-dependent frictional material. The computed results are in good agreement with both the closed-form solutions and displacement-controlled experiments reported in the literature. A parametric study was performed to further investigate the influence of the loading rate, material properties, and heterogeneities on the pressuremeter test simulations.

Keywords: Pressuremeter test, MPM, Cavity expansion.

1 INTRODUCTION

A pressuremeter is an in-situ testing tool performed against the wall of a borehole using a cylindrical probe that is expanded radially [1, 2]. Pressuremeter tests have been used to evaluate soil parameters, such as in-situ shear strength and deformation parameters, offering insights into the mechanical behaviour of geomaterials. It offers several advantages over traditional laboratory tests by directly measuring properties in their natural environment, as well as capturing the effects of true heterogeneity and anisotropy of the material. It is important to note that while many theoretical interpretations of the pressuremeter test idealize it as a cylindrical cavity expansion problem, such simplified assumptions can sometimes introduce significant

errors in the derived soil properties [3]. This discrepancy arises partly due to considering soil as an element and not as a boundary value problem.

Numerical simulations of pressuremeter tests offer a cost-effective, safe, and controlled method to gain insights into soil-pressuremeter interactions and predict soil behaviour under various conditions. However, capturing the nuances of this test within a numerical framework has often been challenged since it is perceived as a large deformation problem. Although effective, numerical techniques in continuum framework, viz. classical Finite Element Methods (FEM), have had their inherent limitations, especially when dealing with the idealization of the test as a cylindrical cavity expansion problem [4]. Actual FEM simulation of pressuremeter tests would usually result in severe mesh distortion issues due to excessive deformation. Within a discrete setting, the simulation of the pressuremeter test in granular material showed promising results when particle shape and friction were considered [5]. Nonetheless, the significant computational cost of DEM can pose an undesirable trade-off, especially when granular-scale micro-mechanical responses are not the primary interest of the study.

The Material Point Method (MPM) is a numerical approach developed within a continuum framework, where Lagrangian particles move through an Eulerian mesh, circumventing mesh distortion problems associated with large deformations. MPM integrates the strengths of continuum mechanics [4] and particle techniques [5], presenting a formidable solution for complex soil-structure interaction scenarios. It has recently garnered attention in the geotechnical engineering community for its ability to address large deformation [6, 7, 8] and the interaction between various materials. One such open-source tool, Anura3D [9], has notably advanced the field by integrating the MPM framework while catering to the specific needs of the geotechnical community. In light of these advancements, this research further explores the use of MPM for the numerical modelling of the pressuremeter test, firstly benchmarking with conventional cylindrical cavity expansion problems and then evaluating its consistency with experimental findings already existing in the literature [10].

2 MPM FORMULATION

We recourse to Anura3D to perform simulations using an explicit 2D axisymmetric MPM model [11] to benchmark the cavity expansion problem. It is further extended to the actual pressuremeter test problem. The following sub-sections provide a detailed exploration of the specific MPM formulation employed in this study.

2.1 Governing Equations

Thermodynamic laws govern a continuum body's behaviour, ensuring mass (Eq. 1), momentum (Eq. 2), and energy (Eq. 3) conservation. In the continuum framework, it is crucial to account for initial and boundary conditions and the material's stress-strain relationship using constitutive equations (Eq. 4). In this study, the explicit MPM dynamic formulation determines acceleration ($\boldsymbol{a}$) from the following equations:

a. *Conservation of Mass:*

$$\frac{d\rho}{dt} + \rho(\nabla . \boldsymbol{v}) = 0 \Rightarrow \frac{dn}{dt} = (1-n)(\nabla . \boldsymbol{v}) \tag{1}$$

Where ρ is the mass density of the material, n is porosity, and $\boldsymbol{v}$ is the velocity of the material.

b. *Conservation of Momentum:*

$$M\boldsymbol{a} = (1-n)\rho_s\boldsymbol{a} = \nabla.\boldsymbol{\sigma}' + (1-n)\rho_s\boldsymbol{b} \tag{2}$$

Where M is the total mass of material, ρ_s is the density of solid grains, $\boldsymbol{\sigma}'$ is an effective stress tensor, and $\boldsymbol{b}$ is a body force vector.

c. *Conservation of Energy:*

$$\rho\frac{dW}{dt} = \dot{\boldsymbol{\varepsilon}}^{\mathrm{T}}\boldsymbol{\sigma} \tag{3}$$

Where W is internal energy per unit mass, $\dot{\boldsymbol{\varepsilon}}^{\mathrm{T}}$ is the transpose of strain rate tensor, and $\dot{\sigma}$ is stress rate tensor.

d. *Constitutive Equation:*

$$\dot{\boldsymbol{\sigma}} = \boldsymbol{D}\dot{\boldsymbol{\varepsilon}} \tag{4}$$

Where $\boldsymbol{D}$ is the stiffness matrix, and the relationship is incremental.

2.2 Comprehensive Process for a Single Calculation Step in 2D Axisymmetric MPM

For a single point (particle) and one phase method in MPM, the computational cycle of each time step (Δt) can be broken down into the following general steps:

a. *Particle-to-Grid Transfer:*

The mass, momentum, and other state variables from the material points (particles) are mapped to the background grid, typically an Eulerian grid.

$$M_i = \sum_{el=1}^{n_{el}}\sum_{mp=1}^{n_{mp,el}} \mathrm{N}^{\mathrm{T}}(\xi_{mp})m_{mp} \tag{5}$$

$$M_i\vec{v}_i = \sum_{el=1}^{n_{el}}\sum_{mp=1}^{n_{mp,el}} \mathrm{N}^{\mathrm{T}}(\xi_{mp})m_{mp}\vec{v}_{mp} \tag{6}$$

Where the subscripts el, i and mp represent the identities of elements, nodes, and material points, respectively, $\mathrm{N}^{\mathrm{T}}(\xi_{mp})$ is the transpose of shape function of element (el) at ξ_{mp} position, n_{el} is the number of elements, $n_{mp,el}$ is the number of material points in el^{th} element, M_i and m_{mp} are the mass of i^{th}node and mp^{th} material point, respectively, while, $\vec{v}_i$ and $\vec{v}_{mp}$ are the velocities of i^{th}node and mp^{th} the material point, respectively.

b. *Compute Grid Forces:*

The internal forces ($\vec{f}_i^{int}$) and any external forces ($\vec{f}_i^{ext}$) are calculated on the grid nodes.

$$\vec{f}_i^{int} = \sum_{el=1}^{n_{el}}\sum_{i=1}^{n_{no,el}}\sum_{mp=1}^{n_{mp,el}} \mathrm{B}^{\mathrm{T}}(\xi_{mp})\sigma_{mp}\Omega_{mp} \tag{7}$$

$$\vec{f}_i^{ext} = \sum_{el=1}^{n_{el}} \sum_{mp=1}^{n_{mp,el}} \left[\mathrm{N}^{\mathrm{T}}(\xi_{mp}) f_{mp}^{ext,trac} + \mathrm{N}^{T}(\xi_{mp}) m_{mp} \vec{g} \Omega_{mp} \right] \quad (8)$$

Where $\mathrm{B}^{\mathrm{T}}(\xi_{mp})$ is the transpose of the gradient of shape function of element (el) at ξ_{mp} position $\vec{g}$ is the gravitational vector, Ω_{mp} is volume associated with mp^{th} material point.

c. *Grid Acceleration Update:*

The forces computed in the previous step are used to update accelerations ($\vec{a}_i^t$) on the grid. This is usually done using Newton's second law.

$$\vec{a}_i^t = (\vec{f}_i^{ext} - \vec{f}_i^{int})/M_i \quad (9)$$

d. *Computing Material Point and Grid Velocity:*

The material point velocity ($\vec{v}_{mp}^{t+\Delta t}$) is updated using an explicit Euler time integration scheme as follows,

$$\vec{v}_{mp}^{t+\Delta t} = \vec{v}_{mp}^t + \Delta t \sum_{i=1}^{n_{no,el}} \mathrm{N}_i(\xi_{mp}^t) \vec{a}_i^t \quad (10)$$

The grid velocity is calculated based on Eq. (6).

e. *Grid Update:*

The nodal positions ($\Delta \vec{u}_i^{t+\Delta t}$), and any other state variables are updated. The updated grid velocities are used to calculate the updated nodal displacements as,

$$\Delta \vec{u}_i^{t+\Delta t} = \vec{v}_i^{t+\Delta t} \Delta t \quad (11)$$

f. *Update Particle Stress/Strain, Volume and Density:*

Using the updated velocities and deformations, the new stress or strain increments ($\Delta \boldsymbol{\varepsilon}_{mp}^{t+\Delta t}$) for the particles are evaluated. This usually involves consideration of the material model and its constitutive behaviour.

$$\Delta \boldsymbol{\varepsilon}_{mp}^{t+\Delta t} = \mathrm{B}_{el}^{\mathrm{T}}(\xi_{mp}^t) \Delta \vec{u}_i^{t+\Delta t} \quad (12)$$

Based on volumetric strain increment ($\Delta \boldsymbol{\varepsilon}_{V,mp}^{t+\Delta t}$), Particle volume ($\Omega_{mp}^{t+\Delta t}$) and mass densities ($\rho_{mp}^{t+\Delta t}$) are updated as follows.

$$\Omega_{mp}^{t+\Delta t} = \Omega_{mp}^t (1 + \Delta \boldsymbol{\varepsilon}_{V,mp}^{t+\Delta t}) \quad (13)$$

$$\rho_{mp}^{t+\Delta t} = \rho_{mp}^t / (1 + \Delta \boldsymbol{\varepsilon}_{V,mp}^{t+\Delta t}) \quad (14)$$

g. *Update Particle Displacements and Positions:*

Using the updated particle strain increment, the new displacements ($\vec{u}_{mp}^{t+\Delta t}$) and positions ($x_{mp}^{t+\Delta t}$) of the particles are computed.

$$\vec{u}_{mp}^{t+\Delta t} = \vec{u}_{mp}^t + \sum_{i=1}^{n_{no,el}} \mathrm{N}_i(\xi_{mp}^t) \vec{u}_i^t \quad (15)$$

$$x_{mp}^{t+\Delta t} = x_{mp}^{t} + \sum_{i=1}^{n_{no,el}} \mathrm{N}_i\left(\xi_{mp}^{t}\right)\vec{u}_i^{t} \tag{16}$$

h. *Grid Reset and Advance to Next Time Step:*

Once all particle information has been updated, the background grid is reset, i.e., all the quantities on the grid are zeroed out for the next time step.

3 BENCHMARKING OF MPM MODEL WITH CYLINDRICAL CAVITY EXPANSION PROBLEM

This section details the MPM numerical modelling scheme used to benchmark the cylindrical cavity expansion problem. To this end, as shown in Figure 1, a cylinder with the cavity is considered. Table 1 presents the cylinder with a cavity with different geometries (cavity radius, outer radius, thickness), material models, and boundary conditions (cavity and external pressures) to be modelled. Due to geometrical symmetry, this problem is modelled using 2D axisymmetric MPM formulation.

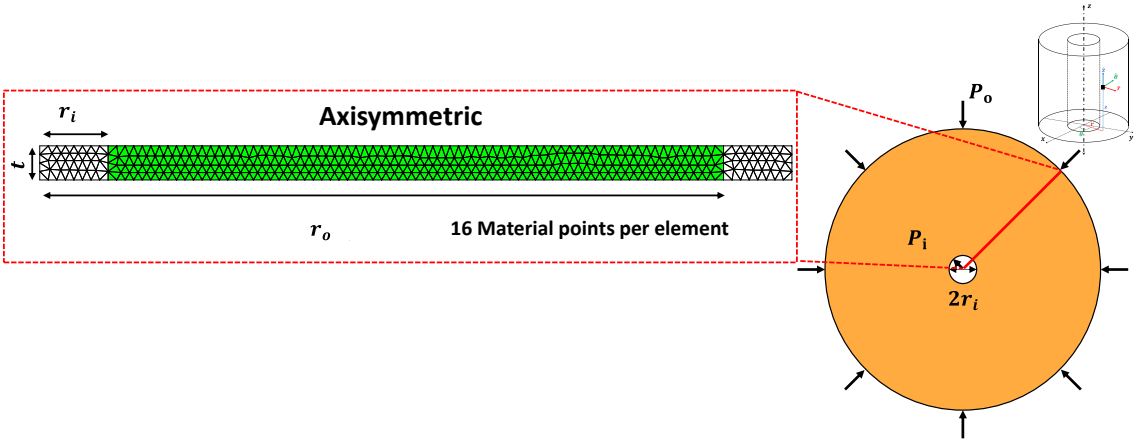

Figure 1: Geometry of the cylinder with cavity; 2D axisymmetric idealization and mesh discretization in MPM (shown in red box).

Table 1: Configurations of cylindrical cavity expansion problem considered for this study.

Case	I	II	III
Geometry			
Cavity radius (r_i)	2 m		2 m
Outer radius (r_o)	20 m		14 m
Thickness (t)	1 m		1 m
Boundary Conditions			
Cavity pressure (P_i)	0	20 MPa	400 KPa
External pressure (P_o)	10 MPa	10 MPa	100 KPa
Material Model	Linear Elastic		Mohr-Coulomb
Young's modulus, E:	70 GPa		70 MPa
Poisson ratio, υ	0.3		0.3
Cohesion, c: kPa	-		1
Ultimate friction angle, φ_u	-		40^0
Ultimate dilation angle, ψ_u	-		-2^0

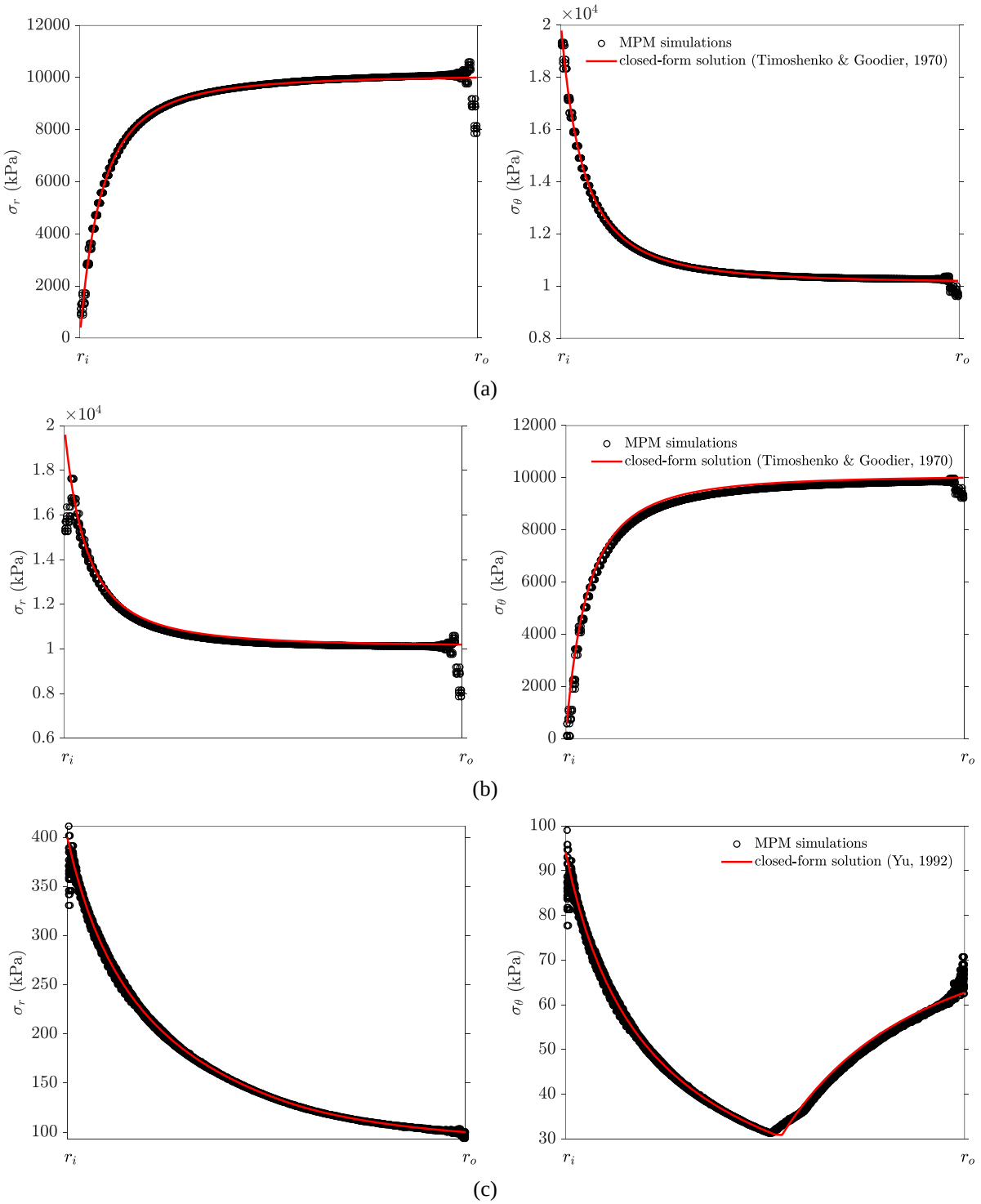

Figure 2: Comparison of radial (σ_r) and circumferential (σ_θ) stresses with radial distance $'r'$ for MPM simulations against closed-form solutions (a) for Case I (b) for Case II; (c) for Case III.

The closed-form solutions of the classical cylinder with cavity problems are available from [12] and [13] for linear elastic and Mohr-Coulomb materials, respectively. The closed-form solutions are automated and solved by implementing routines in MATLAB. Figure 2 shows the variations for radial (σ_r) and circumferential (σ_θ) stress along the radius of the MPM model compared with closed-form solutions. MPM results show high fidelity when compared with the closed-form solutions. In case III, as shown in Figure 2c, MPM simulations can distinguish the formation of plastic and elastic regions.

4 MPM MODELLING OF DISPLACEMENT-RATE CONTROLLED LABORATORY PRESSUREMETER TEST

An experimental study of pressuremeter tests conducted by Fahey [10] using thick cylindrical Leighton Buzzard Sand (LBZ) samples was considered to validate the proposed MPM framework. In the experimental study, the sample, initially having a cavity of 40 mm in diameter, was expanded inside a cylindrical sand specimen with 400 mm in diameter and 200 mm in length. The testing apparatus was designed to maintain a stable boundary pressure of 90 kPa and prevent axial movements. The cavity was expanded to achieve 10% cavity strain, and the corresponding cavity pressure was recorded.

4.1 Geometry, Material model, Boundary conditions and Discretization

We take advantage of the geometrical symmetry of the problem, and thus, half of the geometry is used in MPM 2D axisymmetric simulation. The geometry shown in Figure 3 is a 2D axisymmetric idealization of the experimental program carried out by Fahey [10]. The sand sample has a cavity with a radius r_i = 20 mm, outer radius r_O = 0.2 m and thickness t = 0.2 m is constructed in GiD pre-processor [14], as shown in (Figure 3). LBZ sand is considered a Mohr-Coulomb material with calibrated properties based on [15] listed in Table 2. In MPM simulations, the inside and outside boundary pressures are kept constant (P_o & $P_i = 90\ kPa$) while preventing axial movement as initial conditions. Then, the cavity is expanded radially at a rate of 1 mm/s till a cavity strain of 10% is achieved. The mesh and material point discretization of the MPM model is illustrated in Figure 3. The sixteen material points per element were found to be sufficient to simulate the pressuremeter tests after carrying out a parametric study by varying the number of points per element.

Table 2: Material properties of LBZ sand after [15]

Property	Value
Young's modulus, E: kPa	100000
Poisson ratio, υ	0.25
Cohesion, c: kPa	1
Ultimate friction angle, φ_u	48^0
Ultimate dilation angle, ψ_u	16.5^0

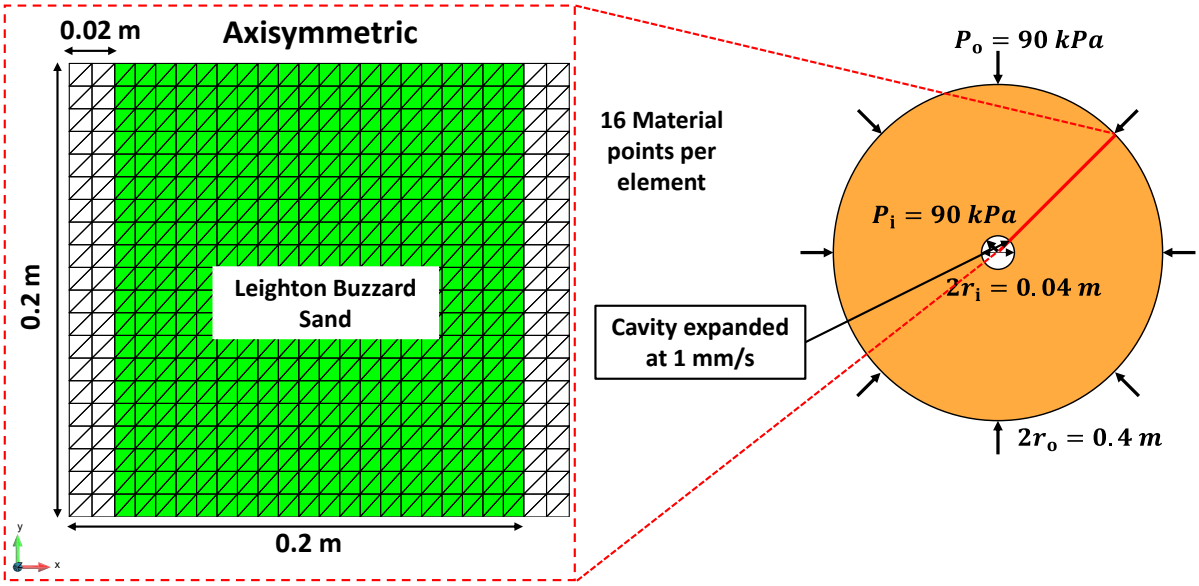

Figure 3: Geometry of displacement-rate controlled laboratory tests [10]; 2D axisymmetric idealization and mesh discretization in MPM (shown in red box).

4.2 Results and Discussions

The displacement profile at the end of the test is shown in Figure 4. Cavity pressure recorded while expanding the cavity to 10% radial strain is achieved was plotted and compared with the experimental results of Fahey [10], as shown in Figure 5. The global response shows good agreement with displacement-controlled laboratory pressuremeter tests. In MPM simulations, a monotonic increase in cavity pressure is observed up to a 4% cavity strain, with maximum cavity pressures ranging between 600-700 kPa sustained until a 10% cavity strain is achieved. In contrast, experimental studies report a maximum cavity pressure of 655 kPa, indicating that MPM simulation results are within ±10% of the experimental findings.

Further insights are gained into the radial stress history during the test. Figure 6 illustrates the evolution of radial stresses (σ_r) at 2.5%, 5%, 7.5%, and 10% cavity strains. Elevated stresses are predominantly localized at the cavity wall, whereas stresses at the external boundary remain unchanged. A uniform radial stress distribution is observed across the thickness of the sample, indicating high fidelity in MPM simulations. Access to such local responses offer advantages over experimental and theoretical interpretations of the pressuremeter test that treat soil as an elemental entity.

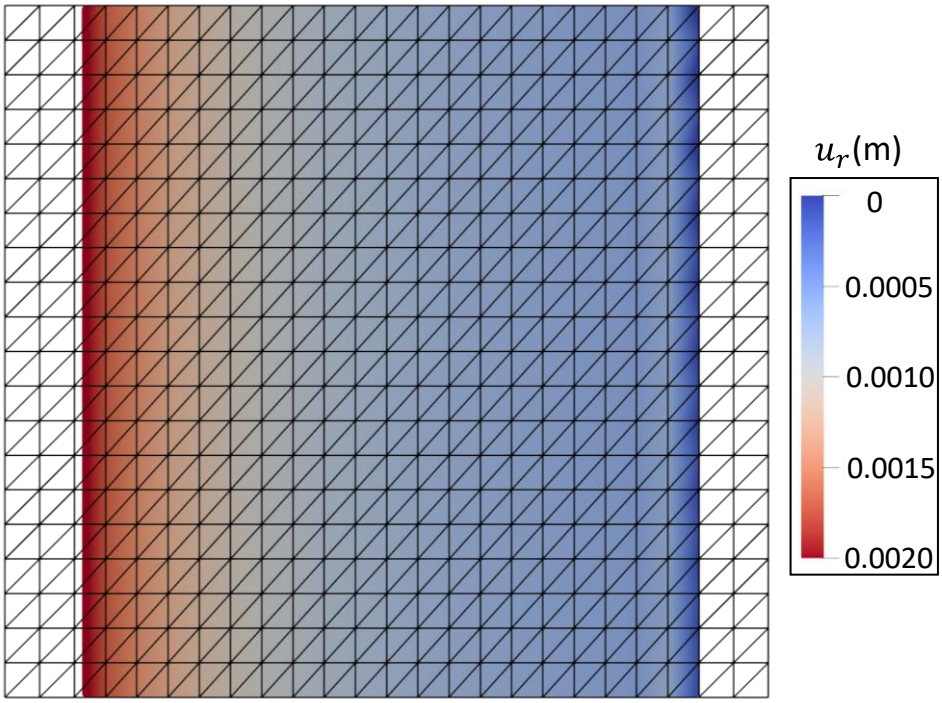

Figure 4: Radial displacement contours of MPM simulations of displacement-rate controlled laboratory pressuremeter tests.

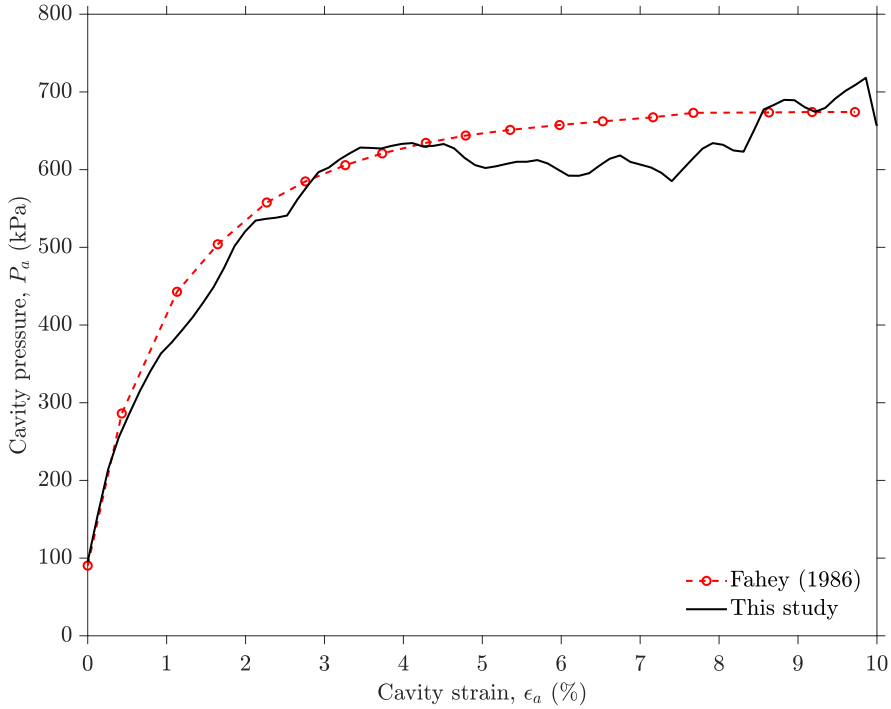

Figure 5: Variation of cavity pressure against cavity strain of MPM simulations compared to experimental studies by [10].

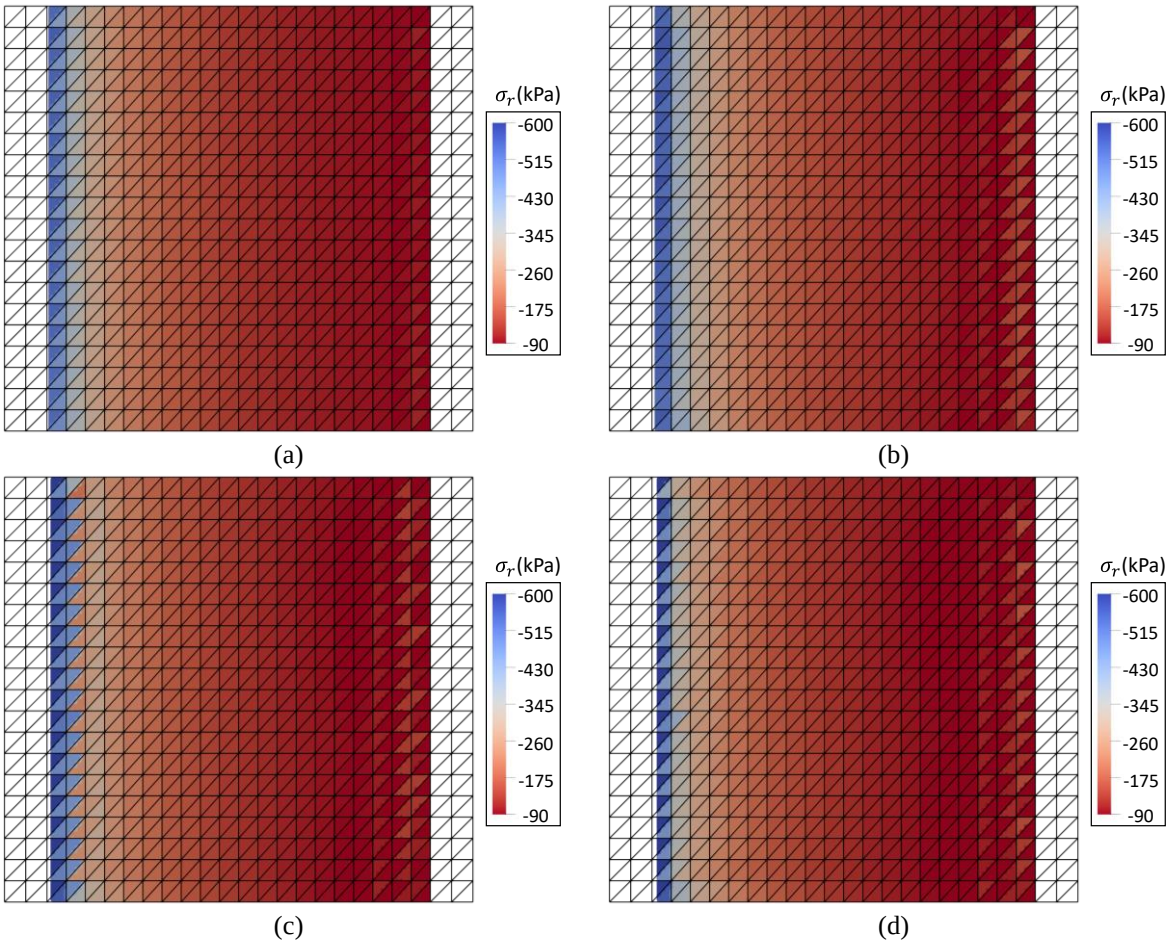

Figure 6: Evolution of radial stress (σ_r) contours of MPM simulations for pressuremeter test at (a) 2.5%, (b) 5%, (c) 7.5%, (d) 10%.

5 CONCLUSIONS

This study investigates the Material Point Method (MPM) as a viable numerical scheme within the continuum framework for simulating the pressuremeter test, a cornerstone in geotechnical in-situ investigations. We utilize the open-source tool, Anura3D, for the MPM simulations and take advantage of the problem's geometrical symmetry to adopt an explicit 2D axisymmetric MPM model. MPM findings are benchmarked against classical cavity expansion problems, highlighting the MPM's efficacy. Further findings of this study can be summarized as follows:

- The global responses from the MPM simulation of the displacement-rate controlled pressuremeter test align with ±10% of the experimental findings.
- MPM simulations can offer insights into localized behaviours, viz. displacement, stress and strain contours, presenting a distinct edge over experimental and theoretical interpretations of the pressuremeter test, which treats soil as a singular element.

The congruence of our results with displacement-controlled experiments from existing literature further underscores the potential of MPM as an indispensable tool in geotechnical

numerical investigations.

REFERENCES

[1] Hughes, J. M. O., Wroth, C. P., & Windle, D. Pressuremeter tests in sands. *Geotechnique* (1977) **27(4):** 455-477.

[2] ASTM D4719-20. Standard test methods for prebored pressure meter testing in soils. *ASTM International* (2020)

[3] Yu, H. S. The First James K. Mitchell Lecture In situ soil testing: from mechanics to interpretation. *Geomechanics and Geoengineering: An International Journal* (2006) **1(3):** 165-195.

[4] Rui, Y., & Yin, M. Interpretation of pressuremeter test by finite-element method. *Proceedings of the Institution of Civil Engineers-Geotechnical Engineering* (2018) **171(2):** 121-132.

[5] Geng, Y., Yu, H. S., & McDowell, G. R. Discrete element modelling of cavity expansion and pressuremeter test. *Geomechanics and Geoengineering* (2013) **8(3):** 179-190.

[6] Soga, K., Alonso, E., Yerro, A., Kumar, K., & Bandara, S. Trends in large-deformation analysis of landslide mass movements with particular emphasis on the material point method. *Géotechnique* (2016) **66(3):** 248-273.

[7] Bisht, V., Salgado, R., & Prezzi, M. Material point method for cone penetration in clays. *Journal of Geotechnical and Geoenvironmental Engineering* (2021). **147(12)**: 04021158.

[8] Yost, K. M., Martinelli, M., Yerro, A., Green, R. A., & de Lange, D. A. Addressing complexities in MPM modeling of calibration chamber cone penetrometer tests in homogenous and highly interlayered soils. *Computers and Geotechnics* (2023) **158:** 105378.

[9] Anura3D MPM Research Community. *Anura3D Version 2022 Source Code* (2022) (www.anura3d.com)

[10] Fahey, M. Expansion of a thick cylinder of sand: a laboratory simulation of the pressuremeter test. *Geotechnique* (1986) **36(3)**: 397-424.

[11] Galavi, V., Tehrani, F. S., Martinelli, M., Elkadi, A. S., & Luger, D. Axisymmetric formulation of the material point method for geotechnical engineering applications. *Numerical Methods in Geotechnical Engineering IX* (2018) 427-434.

[12] Timoshenko, & S. Goodier, J. N., *Theory of elasticity* (1970) McGraw-Hill.

[13] Yu, H. S. Expansion of a thick cylinder of soils. *Computers and Geotechnics* (1992) **14(1)**: 21–41.

[14] Anura3D MPM Research Community. *Anura3D Tutorial Manual version 2022* (2022)

[15] Cavallaro, A., Maugeri, M. & Mazzarella, R. Static and dynamic properties of Leighton Buzzard sand from laboratory tests. *Proceedings of the International conference on recent advances in geotechnical earthquake engineering and soil dynamics* (2001) **10:** 1.13.